The Astrophysical Journal, 803:45 (8pp), 2015 April 10 doi:10.1088/0004-637X/803/1/45

AN OBSERVATIONAL SIGNAL OF THE VOID SHAPE CORRELATION AND ITS LINK TO THE COSMIC WEB

Jounghun Lee[1] and Fiona Hoyle[2]
[1] Astronomy Program, Department of Physics and Astronomy, Seoul National University, Seoul 151-742, Korea; jounghun@astro.snu.ac.kr
[2] Pontifica Universidad Catolica de Ecuador, 12 de Octubre 1076y Roca, Quito, Ecuador; fionahoyle11@gmail.com
Received 2015 November 29; accepted 2015 February 11; published 2015 April 13

ABSTRACT

The shapes of cosmic voids are prone to distortions caused by external tidal forces since their low densities imply a lower internal resistance. This susceptibility of the void shapes to tidal distortions makes them useful as indicators of large-scale tidal and density fields, despite the practical difficulty in defining them. Using the void catalog constructed by Pan et al. from the Seventh Data Release of the Sloan Digital Sky Survey (SDSS DR7), we detect a clear 4σ signal of spatial correlations of the void shapes on a scale of $20\,h^{-1}$ Mpc and show that the signal is robust against the projection of the void shapes onto the plane of sky. By constructing a simple analytic model for the void shape correlation, within the framework of tidal torque theory, we demonstrate that the void shape correlation function scales linearly with the two-point correlation function of the linear density field. We also find direct observational evidence for the cross-correlation of the void shapes with the large-scale velocity shear field that was linearly reconstructed by Lee et al. from SDSS DR7. We discuss the possibility of using the void shape correlation function to break the degeneracy between the density parameter and the power spectrum amplitude and to independently constrain the neutrino mass as well.

Key words: large-scale structure of universe

1. INTRODUCTION

The standard statistics of large-scale structure (LSS), such as the matter density power spectrum, the abundance evolution of galaxy clusters, the galaxy bias function, and the redshift distortion effect, have been prevalently used to probe the initial conditions of the universe. Although the power of the standard LSS statistics as a cosmological probe has been confirmed by numerous observational and numerical studies, its limitation has recently been noted. For instance, Wei et al. (2013) recently proved that standard LSS statistics inherently fail to distinguish between two different cosmological models: coupled dark energy and modified gravity models. In the former, cosmic acceleration is caused by the anti-gravitational effect of scalar field dark energy coupled to dark matter (see Amendola & Tsujikawa 2010, for a review) while the latter attributes the apparent acceleration of spacetime to the deviation of gravity from general relativity on cosmological scales (see Clifton et al. 2012 for a review).

To overcome the limitation of standard LSS statistics, it is necessary to develop as many nonstandard complementary probes as possible. The distribution and correlation of void shapes is one of those nonstandard LSS statistics that has arisen in recent years as a complimentary probe of cosmology (e.g., Park & Lee 2007a; Platen et al. 2008; Lee & Park 2009; Lavaux & Wandelt 2010; Biswas et al. 2010; Bos et al. 2012; Lavaux & Wandelt 2012). The classical work of Icke (1984) predicted that the shape of an isolated void region will become rounder and rounder as its expansion grows faster than the expansion of the rest of the universe. However, it was later pointed out that the cosmic voids should be regarded not as isolated low-density regions but as being in constant interaction with the surrounding matter distribution (van de Weygaert & van Kampen 1993; Dubinski et al. 1993; Sahni et al. 1994). Given that the internal resistance of a region to tidal distortion diminishes with its density, Shandarin et al. (2006) suggested that void shapes should gradually develop nonspherical asymmetry under the tidal shear influence from the surrounding matter distribution.

The statistical link between the non-spherical shapes of cosmic voids and the surrounding tidal shear field have been analytically and numerically investigated by several authors. Noting that the void shapes become most (least) stretched along the direction of the minimum (maximum) external tidal force and that the spatial correlations of the tidal fields would generate the spatial corrections of the void shapes, Lee & Park (2006) introduced the concept of a void spin angular momentum vector to quantify the direction of an asymmetric void shape. Measuring the spatial correlations of the spin axes of the voids identified in an N-body simulation, they found that the numerical result of the void spin correlation matched the analytic prediction based on tidal torque theory. Park & Lee (2007b) found strong alignments between the void spin axes and the elongated axes of the neighbor superclusters identified in an N-body simulation and interpreted this as numerical evidence for tidal influences on the voids shapes, claiming that the shapes of the superclusters would be elongated along the directions of the minimum tidal forces.

Although the new concept of void spin effectively quantifies the influence of the anisotropic tidal field on the void shape, as shown in the pioneering work of Lee & Park (2006), the void spin axis is hard to measure in practice since it requires knowledge of the peculiar velocities of the void galaxies. By quantifying the orientations of the asymmetric void shapes by the distinct principal axes of their inertia momentum, rather than their spin axes, Platen et al. (2008) measured the spatial correlations between the axes of the asymmetric void shapes by analyzing the data from an N-body simulation. They showed that the spatial correlations between the void shapes decrease slowly with separation distance, exhibiting significant correlation strength even on scales larger than $30\,h^{-1}$ Mpc.

However, no direct observational evidence of tidally induced correlations of void shapes has been reported. The main difficulty in dealing with void shapes is over-sensitivity to the

void-identification scheme. Although a variety of void-finding algorithms were compared with one another in the comprehensive work of Colberg et al. (2008), it is still a touchy issue to decide which void finding algorithm is optimal since each algorithm has its own merits and limitations in defining voids and characterizing their properties. Furthermore, the relatively low abundance of observed voids in the local universe hinders performing statistics of void shapes where large numbers of voids are required (e.g., see Bos et al. 2012). Notwithstanding these difficulties, observational confirmation of the theoretical prediction for the link between the void shapes and the tidal shear field is essential to see if statistics of void shapes can be used as a complimentary test of cosmology. The goal of this Paper is to find direct observational evidence for the tidally induced correlations of non-spherical void shapes from recently available large galaxy surveys.

The organization of this paper is as follows. In Section 2, we report a high signal detection of void shape correlations. In Section 3, the observational signals are compared with a simple analytic formula based on the tidal torque theory. In Section 4, we present the first direct observational evidence for cross-correlations between void shapes and the large-scale tidal field. In Section 5, the implications and future applications of our final results are discussed. Throughout this paper, the key cosmological parameters assume values of $\Omega_\Lambda = 0.26$, $\Omega_\Lambda = 0.74$, $h = 0.73$, $\sigma_8 = 0.8$ for a universe dominated by the cosmological constant (Λ) and cold dark matter with Euclidean geometry.

2. DETECTION OF A SIGNAL OF VOID SHAPE CORRELATIONS

To find an observational signal of the void shape correlation, we analyze the void catalog constructed by Pan et al. (2012), who identified low-z voids by applying the void-finding algorithm of Hoyle & Vogeley (2002, HV02 hereafter) to the Seventh Data Release of the Sloan Digital Sky Survey (SDSS DR7; Abazajian et al. 2009). Selecting only those voids with 30 or more member galaxies from the void catalog of Pan et al. (2012), we construct a sample of 831 giant voids whose effective radius ($R_{\rm v}$) and number of member galaxies ($N_{\rm vg}$) are in the ranges of $9.92 \leqslant R_{\rm v} \leqslant 33.92$ and $30 \leqslant N_{\rm vg} \leqslant 2984$, respectively.

It may be worth discussing here the reason for using galaxy voids identified by the HV02 algorithm rather than those by more recent and elaborate void finders like ZOBOV (Neyrinck 2008). First of all, the HV02 algorithm can be readily implemented into the spatial distributions of the observed galaxies from the large-scale survey to identify voids without making any assumption about galaxy bias or halo abundances (see also, Hoyle & Vogeley 2004; Pan et al. 2012) . Second of all, we intend to compare the observed signal of the void shape correlations with an analytic model constructed as a modification of the void spin correlation model of Lee & Park (2006; see Section 3). When Lee & Park (2006) derived their analytic model for the void spin correlation function, they tested it against the numerical result obtained utilizing the HV02 algorithm for an N-body simulation and found good agreement, which motivated us to select the HV02 algorithm for our current analysis.

Using information on the redshifts, right ascensions, and declinations, we first measure the positions of the member galaxies of each void and then determinate the location of its luminosity center, $\boldsymbol{x}^0 = \left(x_i^0\right)$, as

$$\boldsymbol{x}_0 = \frac{\sum_\alpha M_{\rm r}^\alpha \boldsymbol{x}^\alpha}{\sum_\alpha M_r^\alpha}, \tag{1}$$

where $\boldsymbol{x}^\alpha$ is the position of the αth galaxy in a given void and M_r^α is its absolute magnitude in the r band. The inertia momentum tensor of each void, $\boldsymbol{I} = \left(I_{ij}\right)$, is now calculated as (Lee & Park 2006)

$$I_{ij} = \sum_\alpha M_r^\alpha \left(x_i^\alpha - x_i^0\right)\left(x_j^\alpha - x_j^0\right). \tag{2}$$

Diagonalizing $\boldsymbol{I}$ for each void, we find three (orthonormal) eigenvectors (say, $\boldsymbol{u}_1, \boldsymbol{u}_2, \boldsymbol{u}_3$) corresponding to the three eigenvalues (I_1, I_2, I_3 in a decreasing order) and label them as the major, intermediate, and minor principal axes of the void shape, respectively.

Note that the *void shape* in the current work is defined in terms of the spatial positions of the galaxies in a void region relative to their luminosity center, which is different from the true geometry of a void region. Since the void galaxies are located in a relatively denser section of the void region, their luminosity center would deviate from the density minimum of the void region, which is usually defined as the void center. Although the spatial distributions of the void galaxies should develop anisotropy under the influence of the external tidal shear field, the non-spherical geometry of a void region with density minimum as its center should be a better indicator of the external tidal field than the anisotropic spatial distribution of the void galaxies. Unfortunately, however, it is very hard to accurately measure the three-dimensional geometry of a void region from observational data since its boundary depends very sensitively on which void finding algorithm is used (Colberg et al. 2008). To avoid this practical difficulty and to be consistent with Lee & Park (2006), we use the anisotropic spatial locations of the void galaxies to define the void shape and call their luminosity center the void center throughout this paper.

If a void had a spherically symmetric shape, then the three eigenvalues of its inertia momentum tensor would be identical, and thus the corresponding three eigenvectors would be degenerate. The more nonspherical the shape of a void is, the more distinct the three eigenvectors of its inertia momentum tensor are from one another. Measuring two ratios of I_2/I_1 and I_3/I_1 for each void, we find the probability density distributions, $p\left(I_2/I_1\right)$ and $p\left(I_3/I_1\right)$, which are plotted as histograms with Poisson errors in the left and right panels of Figure 1, respectively. As can be seen, the two distributions, $p\left(I_3/I_1\right)$ and $p\left(I_2/I_1\right)$, attain their maxima at $I_3/I_1 \approx 0.4$ and $I_2/I_1 \approx 0.6$, respectively, which shows that the three principal axes of the voids in the sample are quite distinct from one another.

The spatial correlation function of the void shapes, $\eta_{\rm v}(r)$, is defined in a similar way as the spatial correlation function of the halo shapes defined by Lee et al. (2008):

$$\eta_{\rm v}(r) \equiv \left\langle \left|\boldsymbol{u}(\boldsymbol{x}) \cdot \boldsymbol{u}(\boldsymbol{x}+\boldsymbol{r})\right|^2 \right\rangle - \frac{1}{3}, \tag{3}$$

where $\boldsymbol{u}(\boldsymbol{x})$ and $\boldsymbol{u}(\boldsymbol{x}+\boldsymbol{r})$ are the principal axes of two voids located at the positions of $\boldsymbol{x}$ and $\boldsymbol{x}+\boldsymbol{r}$, respectively. In Equation (3), the ensemble average of the first term in the left-hand side is taken over all void pairs in the sample whose

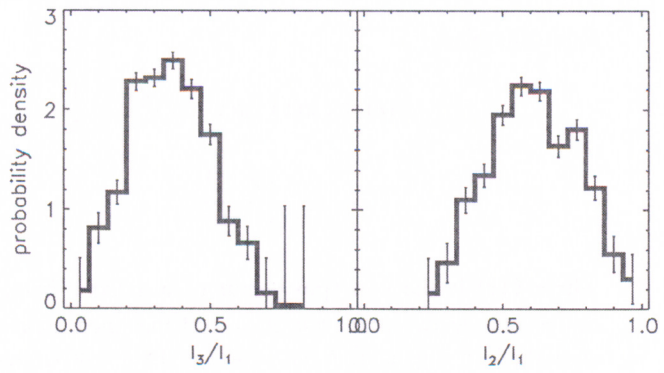

Figure 1. Probability density distributions of the ratios of the smallest (second smallest) eigenvalues to the largest ones of the inertia tensors of the sample voids from SDSS DR7 with Poisson errors in the left (right) panel.

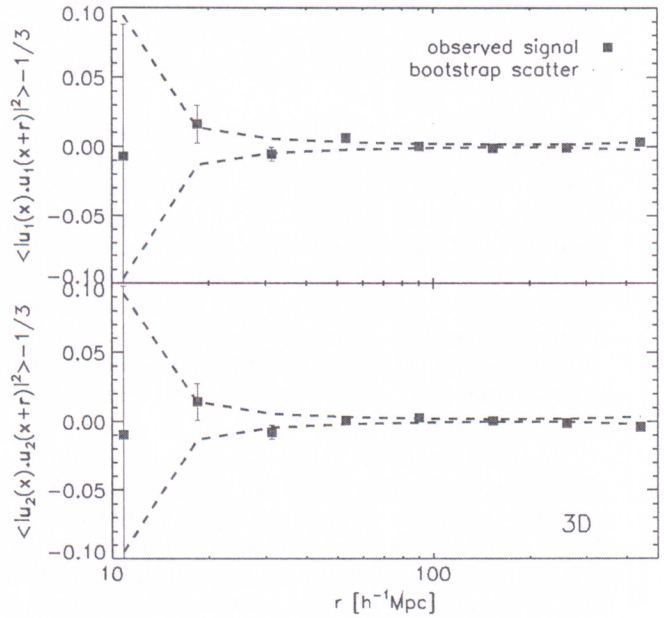

Figure 2. Spatial correlations of the major and intermediate principal axes of the inertia tensors of the sample voids as square dots in the top and bottom panels, respectively. In each panel, the errors represent the one standard deviation in the measurement of the mean correlations, the dotted line corresponds to the case of zero correlation, and the dashed lines show the scatters among the bootstrap 1000 resamples.

separation distance is r, while the second term, 1/3, represents the expectation value of the first term under the null hypothesis of no correlation. Note that $\eta_v(r)$ would be zero if not for correlation.

To determine $\eta_v(r)$, we take the following steps. First, we find the range of separation distances, r, of all pairs from the 831 voids in our sample. Second, we divide the values of r into small bins with size Δr and find those void pairs whose separation distances are in the interval $[r, r + \Delta r]$. Third, we compute the dot-products between the principal axes of the inertia momentum tensors of two voids in each pair and then take the ensemble average over those void pairs whose separation distances belong to each r bin. Fourth, we subtract 1/3 from the ensemble average to obtain η_v and calculate the standard deviation of σ_η in the measurement of η_v at each r bin. Fifth, we estimate the scatters of η_v among 1000 bootstrap resamples.

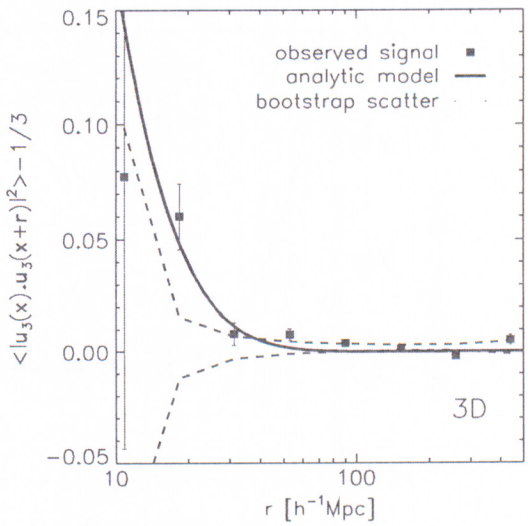

Figure 3. Same as Figure 2 but for the case of the minor principal axes of the void inertia tensors. The solid line represents an analytic model based on the linear tidal torque theory.

Figure 2 shows the spatial correlation function of the major and intermediate principal axes of the void inertia tensors as square dots with one standard deviation error σ_η in the top and bottom panels, respectively. In each panel, the dotted line represents the case of no spatial correlations and the dashed line depicts the bootstrap scatter among 1000 resamples. As can be seen, the major and intermediate principal axes of the void inertia tensors show no signal of spatial correlations. Figure 3 shows the same as Figure 2 but for the case of the minor principal axes of the void inertia tensors. As can be seen, there is a clear signal of spatial correlation as high as $4\sigma_\eta$ at the bin of $r \approx 20\,h^{-1}$ Mpc. At larger separation distances, the correlation signal is not statistically significant, lower than twice the bootstrap error.

To confirm that the observed signal of the spatial correlations of the minor principal axes of the void inertia tensors is not a spurious one generated by some systematic errors involved in the measurements of the galaxy positions in redshift space, we redo the alignment analyses in the two-dimensional plane of sky. For each void, we project the minor principal axes of its inertia tensor along the line-of-sight (LOS) direction to the void center and then determine the spatial correlations of the projected minor principal axes as a function of the separation distance, the result of which is displayed in Figure 4. Here, $\boldsymbol{u}_3^{2d}$ denotes the projected minor principal axes of the void inertia tensors onto the plane of the sky. Note that for the case of no correlation, the ensemble average terms are expected to yield one-half rather than one-third for the case of the projected axes. As can be seen, a correlation signal is still present with almost the same strength at $r \approx 20\,h^{-1}$ Mpc even using projected directions, which verifies that the observed signal of the void shape correlation is truly intrinsic.

It is worth explaining here why only the minor principal axes of void inertia tensors show correlations. Since a void region would become most stretched along the direction of the minimum external tidal force, it might seem natural for us to expect that the major principal axes of the void inertia tensors should be as strongly correlated as their minor counterparts. However, as mentioned above, we define the void shape in terms of the spatial positions of the void galaxies relative to

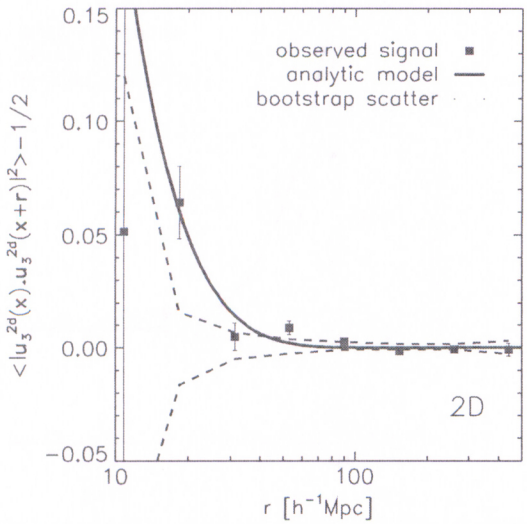

Figure 4. Same as Figure 3, but for the case of the projected minor principal axes onto the two-dimensional plane of sky.

their luminosity centers. The most stretched section of a void region must be the emptiest, being almost devoid of galaxies. Thus, when the void inertia tensor is defined from the locations of the void galaxies, the major principal axis of the inertia tensor should be a poor approximation of the direction of the minimum external tidal force, while its minor axis traces well the direction of maximum external tidal force. In other words, the major principal axes of the void inertia tensors appear to be uncorrelated because they do not trace well the direction of minimum external tidal force, which implies a limitation of our definition of the void shape.

It is interesting to see that our result is consistent with the *N*-body result of Platen et al. (2008), despite several technical differences. In their numerical work with an *N*-body simulation, the watershed void finder developed by Platen et al. (2007) was used to identify matter voids, and void inertia tensors were calculated in terms of the positions and masses of dark matter particles in the voids, whereas in our observational analysis the HV02 algorithm was employed to find galaxy voids, and void inertia tensors were determined by using only luminous void galaxies. The consistency of the observed signal of the void shape correlations presented here with their numerical result implies that the anisotropic spatial distributions of the void galaxies trace the overall non-spherical shapes of matter voids.

3. COMPARISON OF THE OBSERVED SIGNAL WITH AN ANALYTIC MODEL

We now compare the detected signal of the void shape correlations with an analytic model obtained as a modification of the halo shape correlations. Let us first briefly review the analytic models for the galaxy spin and shape correlations developed in previous studies in the framework of tidal torque theory. Pen et al. (2000, hereafter PLS00) developed the following analytic formula for the spatial correlations of the halo spin axes

$$\eta_{\rm g,spin}(r) \equiv \left\langle |\boldsymbol{s}(\boldsymbol{x})\cdot\boldsymbol{s}(\boldsymbol{x}+\boldsymbol{r})|^2 \right\rangle - \frac{1}{3} = \left[\frac{a_{\rm L}}{\sqrt{6}}\frac{\xi_{R_G}(r)}{\xi_{R_G}(0)}\right]^2, \quad (4)$$

where $\hat{\boldsymbol{s}}(\boldsymbol{x})$ is the unit spin vector of a galactic halo, $\xi_{R_G}(r)$ represents the two-point correlation of the linear density field smoothed on a galactic scale of $R_{\rm G} \approx 0.5\,h^{-1}$ Mpc, and $a_{\rm L}$ is the linear correlation coefficient that lies in [0, 3/5] according to the linear tidal torque theory (Doroshkevich 1970; White 1984; Catelan & Theuns 1996; Lee & Pen 2000, 2001; Porciani et al. 2002a, 2002b). PLS00 found fairly good agreement between Equation (4) with an empirical value of $a_{\rm L} \approx 0.1$ and the observed galaxy spin correlations from the nearby universe (see also Lee & Erdogdu 2007; Lee 2011).

The critical aspect of Equation (4), based on linear tidal torque theory, is that the halo spin correlation drops very rapidly with r as it is proportional to the square of the linear density correlation function. In other words, Equation (4) predicts that the signal of the halo spin correlation is significant only on scales of a few Mpc. Follow-up numerical experiments found that the nonlinear evolution of the tidal shear field would induce larger-scale correlations of the halo spin axes and suggested that the halo spin correlation should be described as a linear scaling of ξ_{R_G} (Catelan et al. 2001; Hui & Zhang 2008; Lee & Pen 2008).

The directions of the galaxy spin axes are hard to accurately determine in practice, expect for the case of late-type spiral galaxies for which a thin-disk approximation can be made. Given that the angular momentum of a galactic halo is closely linked to the elongation of its ellipsoidal shape, tidally induced spatial correlations are also expected to be present in the direction of halo shapes which are readily observable in practice. In addition, unlike halo spin axes which are more or less conserved after decoupling of the halos from the tidal shear field, halo shapes do not retain their initial memory after the proto-halos decouple, and thus their spatial correlations are likely to respond much more sensitively to nonlinear growth of the tidal shear field than those of the halo spin axes.

Lee et al. (2008) determined the halo shape correlations by analyzing the Millennium galaxy catalog (Springel et al. 2005) and found them to be well approximated as a linear scaling of ξ_{R_G}:

$$\eta_{\rm g,shape}(r) \equiv \left\langle |\boldsymbol{u}(\boldsymbol{x})\cdot\boldsymbol{u}(\boldsymbol{x}+\boldsymbol{r})|^2 \right\rangle - \frac{1}{3} = a_{\rm L}\frac{\xi_{R_G}(r)}{\xi_{R_G}(0)}, \quad (5)$$

where $\boldsymbol{u}$ represents the principal axes of the halo inertia tensors, which coincide with the directions of their ellipsoidal shapes. Note that there are two differences between Equations (4) and (5). First, the halo shape correlations are proportional to the two-point linear density correlation function while the halo spin correlation is proportional to the square of it, which indicates that the halo shapes possess larger-scale correlations than the halo spin axes. Second, the linear correlation coefficient $a_{\rm L}$ for the halo shape correlation is not reduced by a factor of $\sqrt{6}$,

unlike the case of spin correlation. This results from the fact that halo minor axes are expected to be maximally correlated with the major principal axes of the tidal shear field (e.g, Lee et al. 2008), while halo spin axes are only preferentially correlated with intermediate tidal shear principal axes (Doroshkevich 1970; White 1984; Catelan & Theuns 1996; Lee & Pen 2000; Porciani et al. 2002a, 2002b). These two differences imply that the halo shapes should not only exhibit larger scale but also stronger correlations than the halo spin axes.

Meanwhile, the validity of Equation (4) was extended to the case of void spin, a new concept introduced by Lee & Park (2006) to quantify the effect of the tidal shear field on the dynamics of void galaxies. Given the analytic result of Lee (2006) that the linear correlation coefficient tends to have its maximum value in regions with lowest local density, Lee & Park (2006) suggested that the spatial correlations of the void spin axes could be described by Equation (4) with $a_{\rm L} = 0.6$ (i.e., the maximum value of the linear correlation coefficient):

$$\eta_{\rm v,spin}(r) = \left[\frac{3}{5\sqrt{6}}\frac{\xi_{R_{\rm v}}(r)}{\xi_{R_{\rm v}}(0)}\right]^2, \tag{6}$$

where $\xi_{R_{\rm v}}$ is the two-point correlation function of the linear density field smoothed on a void scale that amounts to the effective Lagrangian radius of a void. Equation (6) was tested against an N-body simulation by Lee & Park (2006) and turned out to work well even though it has no fitting parameter.

In light of the previous works reviewed here, we now suggest that the void shape correlation function $\eta_{\rm v}$ could be described by Equation (5) with a maximum value of $a_{\rm L} = 3/5$:

$$\eta_{\rm v,shape}(r) = \frac{3}{5}\frac{\xi_{R_{\rm v}}(r)}{\xi_{R_{\rm v}}(0)}. \tag{7}$$

For the case of the spatial correlation of the projected void shapes, the proportionality constant changes from 3/5 to 4/5 (see Appendix H in Lee & Pen 2001):

$$\eta_{\rm v}(r) = \frac{3}{4}\frac{\xi_{R_{\rm v}}(r)}{\xi_{R_{\rm v}}(0)}. \tag{8}$$

The solid lines in Figures 3 and 4 represent Equations (7) and (8), respectively, compared with the numerical results (dots) obtained in Section 2. As can be seen, the strengths of the correlation signals detected at a distance bin of $r \approx 20\,h^{-1}$ Mpc shown in Figures 3–4 match well the analytic predictions of Equations (7)–(8).

4. CROSS-CORRELATIONS BETWEEN THE VOID SHAPES AND THE VELOCITY SHEARS

The observational signal of the void shape correlation and its good agreement with the analytic model based on tidal torque theory provides compelling *indirect* evidence for the dominant effect of the tidal shear field on void shapes. It would be tantalizing to detect *direct* observational evidence for a connection between the void shapes and the tidal shears. If the tidal shear forces drive the voids to develop non-spherical shapes, then it is expected that the void shapes will be least stretched in the direction of the maximum gravitational force. In other words, the minor axes of the void inertia tensors are expected to not be isotropically oriented in the principal frame of the local tidal tensors but preferentially aligned with the major principal axes of local tidal tensors.

Tidal shear is identical to velocity shear if the peculiar velocity is calculated as a gradient of the gravitational potential under the assumption of no vorticity. Lee et al. (2014) linearly reconstructed the velocity shear field in the nearby universe over a volume of $180^3\,h^{-3}\,{\rm Mpc}^3$ corresponding to a redshift range of $0 \leqslant z \leqslant 0.08$. The local volume was divided into 256^3 cubic grids, and in each the velocity shear tensors $\Sigma_{ij}(\boldsymbol{x})$ were calculated by analyzing the peculiar velocity field linearly reconstructed by Wang et al. (2012) from samples of galaxies from SDSS DR7 with masses larger than $10^{12}\,h^{-1}\,M_{\odot}$.

By conducting the Fourier transformation of the peculiar velocity field $\boldsymbol{v}(\boldsymbol{x})$ into Fourier space, Lee et al. (2014) calculated the Fourier amplitude, $\tilde{\Sigma}_{ij}(\boldsymbol{k})$, of the velocity shear field smoothed by a Gaussian window on a filtering scale of R_f according to the definition of Hoffman et al. (2012):

$$\tilde{\Sigma}_{ij}(\boldsymbol{k}) = -\frac{1}{2H_0}\left(k_i\tilde{v}_j + k_j\tilde{v}_i\right)\exp\left(-\frac{R_f^2k^2}{2}\right), \tag{9}$$

where $\tilde{\boldsymbol{v}}(\boldsymbol{k}) = \left(\tilde{v}_1, \tilde{v}_2, \tilde{v}_3\right)$ is the Fourier amplitude of the peculiar velocity field. Then, they conducted the inverse Fourier transformation of $\tilde{\Sigma}_{ij}(\boldsymbol{k})$ to determine the velocity shear tensor $\Sigma_{ij}(\boldsymbol{x})$ at each grid point, whose three eigenvectors, corresponding to three eigenvalues, were obtained via the similarity transformation. For a detailed description of the linear reconstruction of the velocity shear field, see Lee et al. (2014).

Among the 843 voids in the sample, we find that only 220 voids are located within the local volume of $180^3\,h^{-3}\,{\rm Mpc}^3$ where the velocity shear field was reconstructed. The grid in which the luminosity center of each selected void belongs is identified and we define the major, intermediate, and minor principal axes of the velocity shear tensor of the grid as its eigenvectors corresponding to the largest, second largest, and smallest eigenvalues. The smoothing scale of the velocity shear tensor is set at $R_f = 5\,h^{-1}$ Mpc, which is close to the mean value of the effective Lagrangian radius of the selected voids (Pan et al. 2012).

Before measuring alignments between the minor axes of the void inertia tensors and the principal axes of the local velocity shear tensors, however, we would like to examine whether or not the principal axes of both tensors are isotropic in their orientations with respect to LOS directions. As is well known, the observational data sets measured in redshift space are likely to be contaminated by LOS systematics. A false signal of alignment between the principal axes of two tensors could be produced if the LOS systematics contaminated the measurements of the two tensors and consequently induced preferential alignments (or anti-alignments) between the (LOS) directions and their principal axes.

We measure the cosine of the angle between the three principal axes of the velocity shear tensors, $\boldsymbol{e}_i$, and LOS direction, $\hat{\boldsymbol{h}}_{\rm los}$, at the luminosity center of each void and then take the average value over the 230 voids located in the local volume as $\langle|\boldsymbol{e}_i \cdot \boldsymbol{h}_{\rm los}|\rangle$. If the shear principal axes are isotropic in their orientatons relative to the LOS directions, then the average value of the cosines of the angles would be 0.5 for all three cases of $\boldsymbol{e}_1$, $\boldsymbol{e}_2$, $\boldsymbol{e}_3$. The left panel of Figure 5 plots the

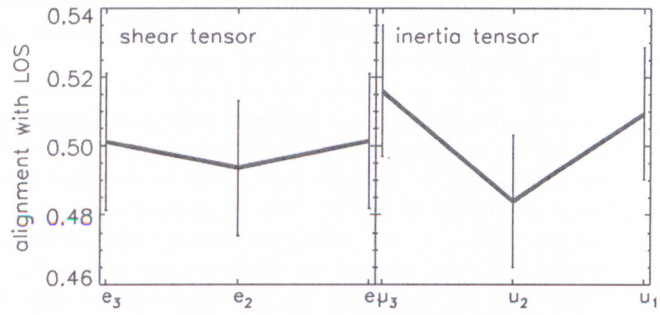

Figure 5. Mean cosines of the angles between the principal axes of the velocity shear (void inertia) tensors and the LOS directions at the centers of the sample voids in the left (right) panel.

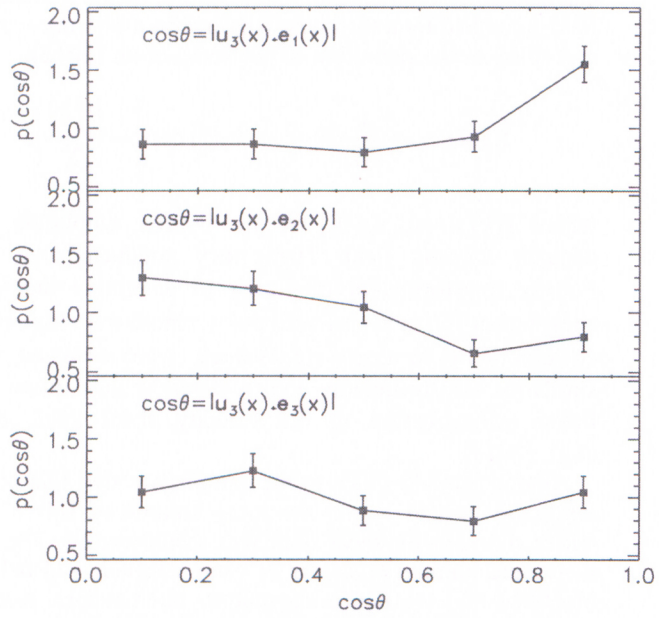

Figure 6. Probability density distributions of the cosines of the angles of the minor principal axes of the void inertia tensors relative to the major, intermediate, and minor principal axes of the velocity shear tensors in the top, middle, and bottom panels, respectively.

results; the errors represent one standard deviation in the measurement of the average. As can be seen, there is no statistically significant signal of alignment between $\boldsymbol{e}_i$ and $\boldsymbol{h}_{\rm los}$. The differences between the resulting average values and the expectation value of 0.5 are all within the statistical errors, indicating that the principal axes of the velocity shear tensors at the luminosity centers of the selected voids are isotropic in their orientations with respect to $\boldsymbol{h}_{\rm los}$. We repeat the same calculation but using the principal axes of the void inertia momentum tensors, $\boldsymbol{u}_i$, and find that their orientations are also isotropic relative to $\boldsymbol{h}_{\rm los}$, as shown in the right panel of Figure 5.

Having confirmed that there is no significant LOS systematics in the measurements of the principal directions of the void inertia and local tidal shear tensors, we now measure the cosine of the angle between the minor principal axis of the void inertia tensor and the three principal axes of the velocity shear tensor at the luminosity center of each selected void as $\cos\theta = |\boldsymbol{u}_3 \cdot \boldsymbol{e}_i|$ for $i = 1, 2, 3$. Binning $\cos\theta$ and counting the voids whose $\cos\theta$ values belong to a given bin, we evaluate the probability density distribution, $p(\cos\theta)$, for $i = 1, 2, 3$. If the minor principal axes of the void inertia tensors are aligned

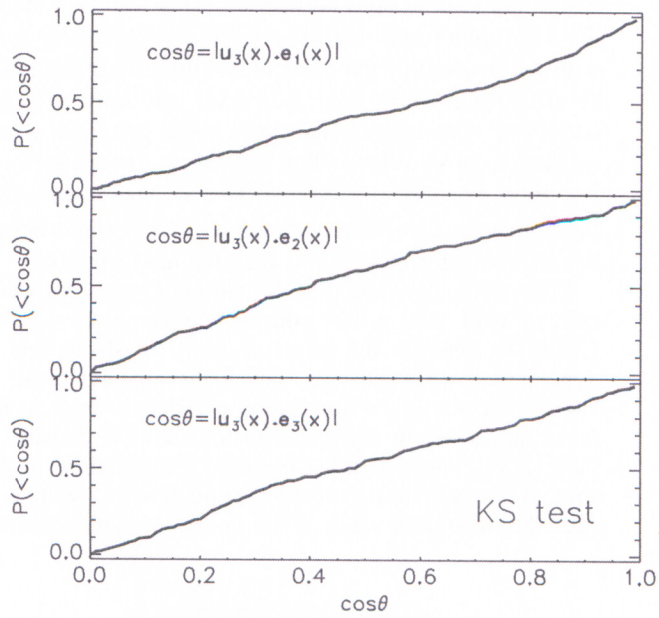

Figure 7. KS tests of the null hypothesis (dotted line) of no correlation between the void inertia and the velocity shear tensors. The lar[illegible]he maximum difference between the cumulative probability, $P(<\cos\theta)$, fr[illegible]the observational data (solid line) and the expectation of the null hypothesis, $P(<\cos\theta) = \cos\theta$, the larger confidence the null hypothesis is rejected at.

(anti-aligned) with the principal axis of the shear tensor, then $p(\cos\theta)$ will show an increase (decrease) with $\cos\theta$.

Figure 6 shows the results as solid squares with Poisson errors. As can be seen, the minor principal axes of the void inertia tensors $\boldsymbol{u}_3$ exhibit a tendency of alignment (anti-alignment) with the major (intermediate) principal axes of the velocity shear tensor $\boldsymbol{e}_1$ ($\boldsymbol{e}_2$), providing *direct* observational evidence for the theoretical claim that void shapes are nonspherical and least stretched along the direction of the maximum tidal force. Note also that no signal of alignment or anti-alignment is found between $\boldsymbol{u}_3$ and $\boldsymbol{e}_3$.

Given that the number of voids, 220, is rather small, we perform a KS test of the null hypothesis of no alignment. If there were no alignments between the principal axes of the two tensors, then the probability $p(\cos\theta)$ would be unity, or equivalently the cumulative probability, $P(<\cos\theta)$, [illegible]d equal $\cos\theta$. Comparing this expectation value of $\cos\theta$ with the observed cumulative probabilities $P(<\cos\theta)$, we find the largest differences between the two, $|P(<\cos\theta) - \cos\theta|$, to be 0.120, 0.121, 0.075 for the cases $\boldsymbol{e}_1$, $\boldsymbol{e}_2$, $\boldsymbol{e}_3$, respectively. The results are shown in Figure 7. According to the KS sample test with 220 data points (Wall & Jenkins 2012), the null hypotheses of no alignment between $\boldsymbol{u}_3$ and $\boldsymbol{e}_1$ and no anti-alignment between $\boldsymbol{u}_3$ and $\boldsymbol{e}_2$ are rejected at the 99.8% and 99.9% confidence levels, respectively.

We repeat the entire process described above for three different filtering scales: $R_f = 3, 7, 10\,h^{-1}$ Mpc. Figure 8 shows how the probability density distributions of the cosines of the angles between $\boldsymbol{u}_3$ and $\boldsymbol{e}_1$ change with R_f. As can be seen, the distribution of $p(\cos\theta)$ does not show a large difference in its behavior among the four different cases of R_f. However, we also note that the increment of $p(\cos\theta)$ with $\cos\theta$ becomes shallower when $R_f = 10\,h^{-1}$ Mpc. Although it would be interesting to investigate at what scale of R_f the alignment tendency would disappear, this issue cannot be addressed in the

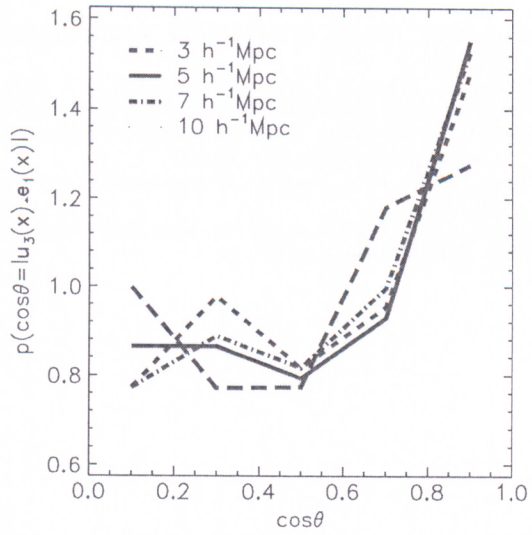

Figure 8. Probability density distributions of the cosines of the angles between the minor principal axes of the void inertia tensors and the major principal axes of the velocity shear tensors for four different cases of the filtering scales.

current work because the validity of the reconstructed velocity shear field will break down when the smoothing scale becomes larger than $10\,h^{-1}$ Mpc due to the boundary effect (Wang et al. 2012).

5. SUMMARY AND DISCUSSION

We have measured the spatial correlations of the principal axes of the inertia tensors of the galaxy voids from SDSS DR7 and detected a clear signal as high as 4σ for the case of minor principal axes on a scale of $20\,h^{-1}$ Mpc. The observed signal has been found to be robust against the projection of the principal axes of the void inertia tensors onto the plane of sky, verifying that the redshift-space distortions have little contamination effect on the directions of the minor principal axes of the void inertia tensors, which is consistent with previous works (e.g., see Foster & Nelson 2009). By constructing a simple analytic model with no fitting parameter for the void shape correlation function based on tidal torque theory, and by comparing the observed signal with the analytic model, we have shown that the observed signal matches the predicted value fairly well.

We have also presented direct observational evidence for the anisotropic orientations of the void shapes in the principal frame of the local velocity shear tensors that were linearly reconstructed from the peculiar velocity field obtained from the galaxy group catalog of the SDSS DR7. It has been found that the minor principal axes of the void inertia tensors are indeed preferentially aligned with the major principal axes of the local velocity tensors. Since the tidal shear field is identical to the linearly reconstructed velocity shear field, this result agrees well with the theoretical expectation that the void shapes stretch least in the directions of the maximum tidal torque forces. The alignment tendency is robust against the change of the filtering scale on which the local velocity field is smoothed, albeit showing a mild decrease as R_f reaches $10\,h^{-1}$ Mpc. Performing the KS test, we reject the null hypothesis of no correlation between the void shapes and the local tidal shear tensors at 99.9% confidence level.

Given that the rescaled linear density correlation function $\xi(r)/\sigma$ is almost independent of the normalization amplitude σ_8 but is still sensitive to the matter density parameter Ω_m, we suggest that the void shape correlation function should be useful for breaking the $\Omega_m - \sigma_8$ degeneracy when combined with the other LSS statistics. The void shape correlation function is also expected to provide an independent constraint on the neutrino mass μ_ν since the behavior of $\xi(r)/\sigma$ would change with an increase of m_ν in the large-scale tail. However, the detection of the void shape correlation has only been successfully detected at one distance bin of $20\,h^{-1}$ Mpc due to the limited numbers of low-z voids, and thus should be regarded as marginal. To use the void shape correlation as a probe of cosmology, however, it will be necessary to overcome the small number statistics by exploring high-z voids and tracing the evolution of the void shape correlations. Our future work is focused in this direction.

We thank the anonymous referee for helpful comments. This work was initiated during the workshop on "Cosmic Voids in the Next Generation of Galaxy Surveys" held at the Ohio State University's Center for Cosmology and Astro-Particle Physics from 2014 August 18–20. We thank P. Sutter and the other organizers of the workshop for making interactactions between participants possible during the workshop. J.L. thanks H. Wang for providing the data set of the reconstructed peculiar velocity field. J.L. was supported by a research grant from the National Research Foundation of Korea to the Center for Galaxy Evolution Research (No. 2010-0027910) and a grant by the Basic Science Research Program through the National Research Foundation of Korea (NRF) funded by the Ministry of Education (No. 2013004372). F.H. acknowledges the support of a PUCE research grant.

REFERENCES

Abazajian, K. N., Adelman-McCarthy, J. K., Agüeros, M. A., et al. 2009, ApJS, 182, 543
Amendola, L., & Tsujikawa, S. 2010, Dark Energy (Cambridge: Cambridge Univ. Press)
Biswas, R., Alizadeh, E., & Wandelt, B. D. 2010, PhRvD, 82, 023002
Bos, E. G. P., van de Weygaert, R., Dolag, K., & Pettorino, V. 2012, MNRAS, 426, 440
Catelan, P., & Theuns, T. 1996, MNRAS, 282, 436
Catelan, P., Kamionkowski, M., & Blandford, R. D. 2001, MNRAS, 320, L7
Clifton, T., Ferreira, P. G., Padilla, A., & Skordis, C. 2012, PhR, 513, 1
Colberg, J. M., Pearce, F., Foster, C., et al. 2008, MNRAS, 387, 933
Doroshkevich, A. G. 1970, Afz, 6, 581
Dubinski, J., da Costa, L. N., Goldwirth, D. S., Lecar, M., & Piran, T. 1993, ApJ, 410, 458
Foster, C., & Nelson, L. A. 2009, ApJ, 699, 1252
Hoyle, F., & Vogeley, M. S. 2002, ApJ, 566, 641
Hoyle, F., & Vogeley, M. S. 2004, ApJ, 607, 751
Hoffman, Y., Metuki, O., Yepes, G., et al. 2012, MNRAS, 425, 2049
Hui, L., & Zhang, J. 2008, ApJ, 688, 742
Icke, V. 1984, MNRAS, 206, 1P
Lavaux, G., & Wandelt, B. D. 2010, MNRAS, 403, 1392
Lavaux, G., & Wandelt, B. D. 2012, ApJ, 754, 109
Lee, J. 2006, ApJL, 644, L5
Lee, J. 2011, ApJ, 732, 99
Lee, J., & Erdogdu, P. 2007, ApJ, 671, 1248
Lee, J., & Park, D. 2006, ApJ, 652, 1
Lee, J., & Park, D. 2009, ApJL, 696, L10
Lee, J., & Pen, U.-L. 2000, ApJL, 532, L5
Lee, J., & Pen, U.-L. 2001, ApJ, 555, 106
Lee, J., & Pen, U.-L. 2008, ApJ, 681, 798
Lee, J., Rey, S.-C., & Kim, S. 2014, ApJ, 791, 15
Lee, J., Springel, V., Pen, U.-L., & Lemson, G. 2008, MNRAS, 389, 1266
Neyrinck, M. C. 2008, MNRAS, 386, 2101

Pan, D. C., Vogeley, M. S., Hoyle, F., Choi, Y.-Y., & Park, C. 2012, MNRAS, 421, 926
Park, D., & Lee, J. 2007a, PhRvL, 98, 081301
Park, D., & Lee, J. 2007b, ApJ, 665, 96
Pen, U.-L., Lee, J., & Seljak, U. 2000, ApJL, 543, L107
Platen, E., van de Weygaert, R., & Jones, B. J. T. 2007, MNRAS, 380, 551
Platen, E., van de Weygaert, R., & Jones, B. J. T. 2008, MNRAS, 387, 128
Porciani, C., Dekel, A., & Hoffman, Y. 2002a, MNRAS, 332, 325
Porciani, C., Dekel, A., & Hoffman, Y. 2002b, MNRAS, 332, 339
Sahni, V., Sathyaprakah, B. S., & Shandarin, S. F. 1994, ApJ, 431, 20
Shandarin, S., Feldman, H. A., Heitmann, K., & Habib, S. 2006, MNRAS, 367, 1629
Springel, V., White, S. D. M., Jenkins, A., et al. 2005, Natur, 435, 629
van de Weygaert, R., & van Kampen, E. 1993, MNRAS, 263, 481
Wall, J. V., & Jenkins, C. R. 2012, Practical Statistics for Astronomers (Cambridge: Cambridge Univ. Press)
Wang, H., Mo, H. J., Yang, X., & van den Bosch, F. C. 2012, MNRAS, 420, 1809
Wei, H., Liu, J., Chen, Z.-C., & Yan, X.-P. 2013, PhRvD, 88, 043510
White, S. D. M. 1984, ApJ, 286, 38